Two-dimensional electrons in lateral magnetic superlattices

I. S. Ibrahim and F. M. Peeters*
Departement Natuurkunde, Universiteit Antwerpen (UIA), Universiteitsplein 1, B-2610 Antwerpen, Belgium
(Received 19 July 1995)

The properties of electrons moving in two dimensions under the influence of a perpendicular magnetic-field of arbitrary strength and which is periodic in one direction are investigated. The magnetic-field modulation is such that the average magnetic-field strength is zero. Four different situations are considered: (1) a magnetic Kronig-Penney system in which the magnetic-field profile consists of a periodic array of δ functions with alternating sign, (2) a periodic array of magnetic-field steps, (3) a sinusoidal magnetic-field profile, and (4) a sawtooth magnetic-field profile. In contrast with the usual potential modulated case, the present systems are not separable and are inherently two dimensional. We found that the energy spectrum consists of magnetic minibands. With the different regions of the energy spectrum we are able to associate particular classical trajectories of the electrons. The density of states and the different components of the conductivity tensor are calculated and exhibit a rich structure due to the presence of the magnetic minibands.

I. INTRODUCTION

The wealth of new and interesting information characterizing the behavior of a two-dimensional electron gas (2DEG) subjected to a perpendicular homogeneous magnetic-field has, in recent years, provided the stimulus for exploring the nonhomogeneous field regime. In Ref. 1 a 2DEG was investigated under the influence of a magnetic step, magnetic-well, and magnetic barrier, and the tunneling of electrons in more complicated systems was found to have interesting wave-vector-dependent properties.[2] Related to this subject is the work of Ramaglia *et al.*[3] who investigated the effect of a local magnetic-field on the tunneling current through a thick potential barrier. The magnetic-field was localized strictly within the potential barrier, which led to resonances that were centered within the barrier. Müller[4] considered an infinite strip of 2DEG in a magnetic-field that varies linearly across the strip and showed that the system has a time-reversal asymmetry and that charge flow takes place only in the direction perpendicular to the field gradient. Calvo[5] analyzed the problem of a 2DEG in a smooth magnetic barrier geometry of different shape and found that the discrete and the continuum energy spectra of such a system overlap. Foden *et al.*[6] investigated electronic transport in a curved 2DEG. In such a system the application of a uniform magnetic-field results in an effective nonuniform magnetic-field. As a consequence, for the case of a cylinder, those authors predicted effective one-dimensional (1D) transport.

A number of papers[7–9] considered quantum transport of a 2DEG in a unidirectional weak magnetic-field modulation where commensurability effects come into play. In most of the latter cases the magnetic-field is modeled by a small sinusoidal component on top of a constant background. This modulation was taken to be small such that one can use perturbation methods to obtain the energy spectrum [7]. Recently, this system was realized experimentally[10] and the predicted [7] semiclassical commensurability effect, which occurs when the classical cyclotron diameter equals an integer number of periods of the potential, up to an additive constant phase factor, were observed.

In this paper we carry the works of Refs. 1 and 7 a step further and study the case in which we have a magnetic field of arbitrary strength that is periodic in one direction. The difference with Ref. 7 is that here there is no uniform background field and consequently the average magnetic field is zero. This implies that electron states can be extended. Furthermore, in contrast to Ref. 7 perturbation theory cannot be used. Recently, the problem of the motion of ballistic electrons in nonhomogeneous magnetic fields has become important for the composite fermion picture of the fractional quantum Hall effect (FQHE). For a density modulated 2DEG, which is in the FQHE regime, the problem can be mapped into that of ballistic motion of composite fermions moving in a periodic magnetic field.[11,12]

The experimental system that we have in mind is one in which a ferromagnetic thin film is deposited on a heterostructure and patterned such that the magnetic domains consist of parallel strips with magnetization perpendicular to the thin film and that change sign from one strip to the next. The magnetic-field emerging from the patterned film will interact with the carriers in the underlying semiconductor structure. This physical system is sketched in Fig. 1(a) together with the corresponding magnetic-field profiles [Fig. 1(b)] in the plane of the 2DEG for different distances z_0 between the ferromagnetic thin film and the 2DEG (see also Ref. 13). The calculation of this magnetic-field profile is given in the Appendix. An alternative route might be through the integration of lithographically patterned superconducting materials on top of the heterostructure. When submerged in a magnetic field this produces a periodic mag-

netic field profile at the 2DEG. But in this case $\langle B \rangle \neq 0$ and such cases will not be considered here. A different technique was used recently, by Leadbeater *et al.*[14] who applied regrowth technology on a substrate in which a series of facets were etched in order to vary the topography of the 2DEG. When a magnetic field is applied to such a shaped 2DEG, the angle between the field direction and the normal to the 2DEG depends on the facet direction. This leads to different shapes of the normal magnetic field profile. A periodic area of such facets results into a periodic effective magnetic field for the 2DEG.

In this work four different magnetic field profiles are considered: (1) magnetic Kronig-Penney system, (2) periodic array of magnetic steps, (3) a sinusoidal magnetic field profile, and (4) a sawtooth magnetic field profile. In all of these cases the total average magnetic field over the whole 2DEG plane is zero.

This paper is organized as follows. Section II gives a short overview of the general problem of periodic magnetic fields. In Secs. III–VI the energy spectrum for each of the considered systems is given. The density of states and electric conductivities are presented in Sec. VII. Our conclusions are presented in the last section.

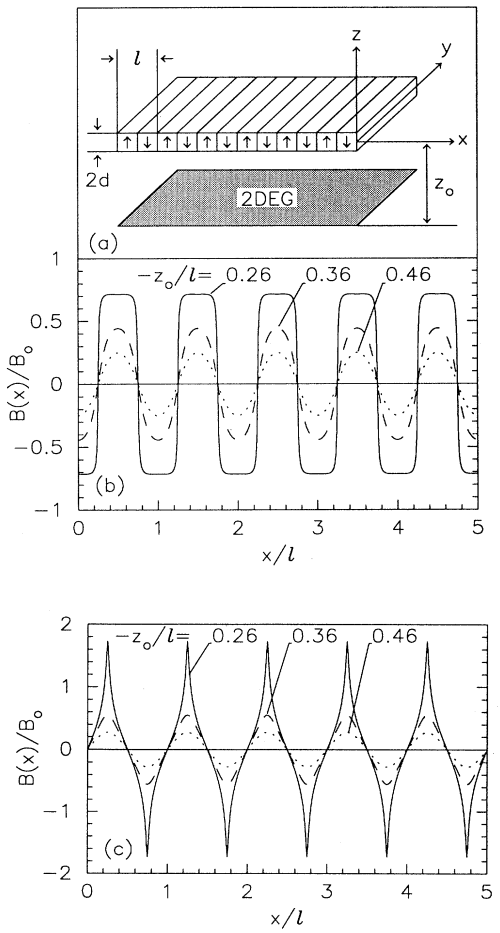

FIG. 1. The proposed physical system (a) and the resulting magnetic-field profiles $B(x)$ in the plane of the 2DEG (b), for different setback distances of the 2DEG. In (c) the magnetic field profiles in the 2DEG are shown in the case the ferromagnetic strips have in-plane magnetization along the x direction but alternating in sign.

II. PERIODIC MAGNETIC FIELDS

Consider electrons moving in a two-dimensional (2D) plane (x, y) in the presence of a perpendicular magnetic field (along the z direction). The magnetic field is taken homogeneous along the y axis and varies along the x axis. Such a magnetic field $\mathbf{B} = \nabla \times \mathbf{A}$ is described, in the Landau gauge, by the vector potential $\mathbf{A} = [0, A(x), 0]$. In the single-particle approximation, the Hamiltonian describing such a system is

$$H = \frac{1}{2m}\left(\mathbf{p} + \frac{e}{c}\mathbf{A}\right)^2 = \frac{1}{2m}\left(p_x^2 + \left[p_y + \frac{e}{c}A(x)\right]^2\right) , \tag{1}$$

where m is the mass of the electron and $-|e| = e$ its charge. Since the y component of the free-electron momentum operator commutes with the Hamiltonian, i.e., $[H, p_y] = 0$, the problem is translational invariant along the y direction and the corresponding wave vector k_y is a conserved quantity. Therefore, the wave function can be written as a product:

$$\Psi(x, y) = e^{ik_y y}\psi(x) \ , \tag{2}$$

where $\hbar k_y$ is the expectation value of p_y in the y direction. The wave function $\psi(x)$ satisfies the one-dimensional (1D) Schrödinger equation

$$\left\{\frac{d^2}{dx^2} - \left[k_y + \frac{e}{\hbar c}A(x)\right]^2 + \frac{2mE}{\hbar}\right\}\psi(x) = 0. \tag{3}$$

Let us introduce the cyclotron frequency $\omega_c = eB_0/mc$ and the magnetic length $\ell_B = \sqrt{\hbar c/eB_0}$ where B_0 is some typical magnetic field strength in the problem. We express all quantities in dimensionless units: (1) the magnetic field $B(x) \to B_0 B(x)$, (2) the vector potential $A(x) \to B_0 \ell_B A(x)$, (3) the time $t \to t\omega_c$, (4) the position coordinate $\mathbf{r} \to \ell_B \mathbf{r}$, (5) the velocity $\mathbf{v} \to \ell_B \omega_c \mathbf{v}$, and (6) the energy $E \to \hbar\omega_c E$. For GaAs and an estimated $B_0 = 0.1T$ we have $\ell_B = 813$ Å, $\hbar\omega_c = 0.17$ meV, and $\ell_B\omega_c = 1.4$ m/sec.

The above Schrödinger equation can now be written in the dimensionless form

$$\left\{\frac{d^2}{dx^2} + 2E - 2V(x, k_y)\right\}\psi(x) = 0, \tag{4}$$

with the expression

$$V(x, k_y) = [k_y + A(x)]^2/2 \ , \tag{5}$$

which can be interpreted as a k_y-dependent effective potential. Note that the effective potential for electron mo-

tion in the x direction depends on the electron wave vector for motion in the y direction. The magnetic field can also be expressed as $B(x) = [dV(x,k_y)/dx]/\sqrt{2V(x,k_y)}$.

In Refs. 1 and 2 the above problem was studied for $B(x)$ profiles of finite extent in the x direction. Here we will investigate $B(x)$ profiles that are periodic in x and such that $\langle B(x)\rangle = 0$. The resulting potential is therefore periodic $V(x,k_y) = V(x+nl,k_y)$ with period l and consequently it is sufficient to find the solution only in one period and use Bloch's theorem to propagate this solution throughout the lattice. The total wave function for the 2D electrons, up to a normalization factor, is given by $\Psi_{n,\mathbf{k}}(\mathbf{r}) = e^{i\mathbf{k}\cdot\mathbf{r}}\psi_{n,\mathbf{k}}(x)$ where $\mathbf{r} = (x,y)$, $\mathbf{k} = (k,k_y)$, and $\psi_{n,\mathbf{k}}(x)$ is the Bloch function, which can be expressed in terms of the solutions of Eq. (4) with band index n and 2D wave vector $\mathbf{k}$. Here k is the Bloch electron wave vector in the x direction. Note that because l is expressed in units of ℓ_B, increasing the period l at constant B_0 is equivalent to increasing the strength of the magnetic field B_0 for a fixed period l.

III. THE MAGNETIC KRONIG-PENNEY MODEL

The solid curve of the magnetic field profile in Fig. 1(c) is modeled by a series of equally spaced δ functions with alternating sign along the x axis: $B(x)/B_0 = \sum_{n=-\infty}^{+\infty}(-1)^n\delta(x-nl/2)$ (see Fig. 2). This is the magnetic analogue of the well-known electrostatic Kronig-Penney model (EKP) and we will call it here the *magnetic Kronig-Penney model* (MKP).[15,16] The vector potential is a step function and can be taken as

$$A(x)/A_0 = \tfrac{1}{2}\mathrm{sgn}[\sin(2\pi x/l)]. \qquad (6)$$

The resulting effective potential (5) is also steplike and is depicted in Fig. 2 for two different values of the wave vector: (i) $k_y = -1.5$ (solid curve), and (ii) $k_y = 2$ (dashed curve). The solution of the Schrödinger equation (4) with this potential (5) consists of plane waves in the well and the barrier regions when the energy $E > V_{\max}$, where $V_{\max} = (|k_y| + 1/2)^2/2$ is the barrier height. Requirements of the continuity of the wave function and its first derivative at the edges of the unit cells and imposing the Bloch periodicity on the wave-function results in the following relation between the electron energy E and its wave vector $\vec{k} = (k,k_y)$

$$\cos(kl) = \cos(\alpha l/2)\cos(\beta l/2) - [(\alpha^2+\beta^2)/(2\alpha\beta)]\sin(\alpha l/2)\sin(\beta l/2)\ , \qquad (7)$$

with $\alpha = \sqrt{2E-(k_y+1/2)^2}$ and $\beta = \sqrt{2E-(k_y-1/2)^2}$. For $E < V_{\max}$ it is to be understood that α becomes imaginary and the corresponding trigonometric functions sin and cos have to be replaced by their hyperbolic counterparts sinh and cosh. The above relation (7) has the same analytic form as the one for the classical EKP system with the difference that here there is an explicit dependence on k_y in the potential and consequently also in the dispersion relation. The latter emphasizes the fact that the problem is essentially two dimensional in nature.

The potential $V(x,k_y)$ is shown in Fig. 3, where it is apparent that as $|k_y|$ increases the wells become deeper (depth= $V_{\max} - V_{\min} = |k_y|$). Accordingly, in the limit $|k_y| \to \infty$ the energy spectrum will approach that of the infinite quantum well. Note also that, in marked contrast with the EKP system, the profile for $V(x,k_y)$ becomes flat at $k_y = 0$, and Eq. (7) reduces to the simple form $E = (k^2+1/4)/2$, implying that motion in the x direction is free and there are no band gaps in the spectrum. This is apparent in Figs. 4-6 where we show the numerical so-

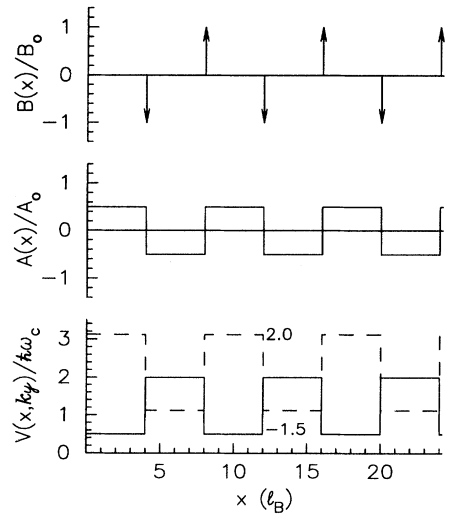

FIG. 2. The profiles for the magnetic field $B(x)$, the vector potential $A(x)$, and $V(x,k_y)$ for $k_y = 2$ (dashed) and $k_y = -1.5$ (solid) for the magnetic Kronig-Penney system.

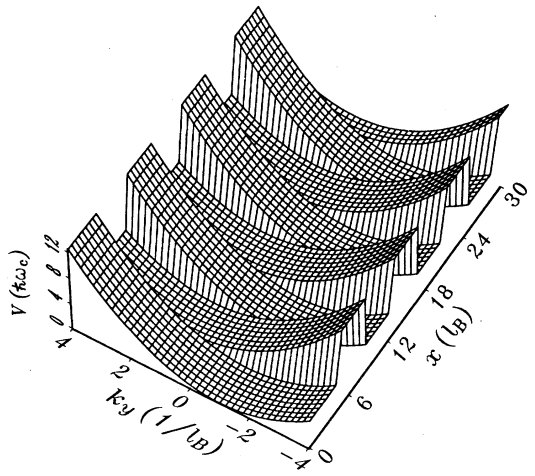

FIG. 3. The effective potential $V(x,k_y)$ for the magnetic Kronig-Penney system with period $l = 8$.

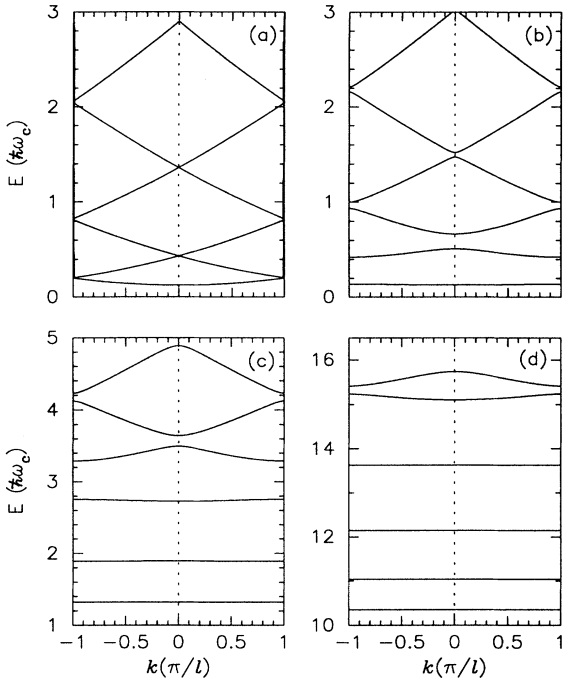

FIG. 4. Energy vs k dispersion curves for $l = 8$ and (a) $k_y = 0$, (b) $k_y = 0.5$, (c) $k_y = 2.0$ and (d) $k_y = 5.0$. Only the lowest six bands are shown.

lution of Eq. (7) for E versus k (Fig. 4), E versus k_y (Fig. 5) and E versus l (Fig. 6). The energy as a function of the wave vector k for motion perpendicular to the superlattice potential (Fig. 4) has the usual appearance of energy

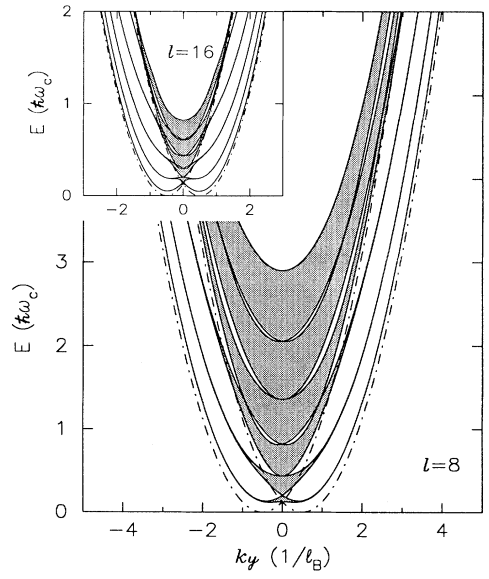

FIG. 5. Energy vs k_y dispersion relation for the MKP system with period $l = 8$. The shaded regions are the lowest six allowed energy bands. The dash-dotted curves show the maxima and minima of $V(x, k_y)$. Inset: The same for $l = 16$.

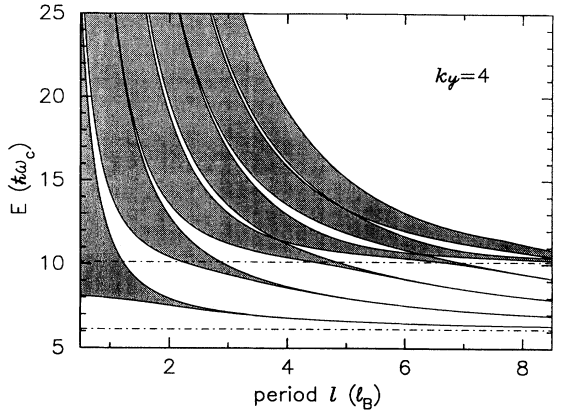

FIG. 6. Energy vs period l for a fixed $k_y = 4$. The shaded regions are the allowed energy bands of which only the lowest six are shown. The dash-dotted lines are the maxima and minima of $V(x, k_y)$.

minibands in which allowed energy bands are separated by forbidden gaps. The widths of the bands and the gaps between them depend on k_y, which is not so in the case of the EKP system. In the latter the Schrödinger equation is separable and the energy spectrum has the form $E_n(k, k_y) = E_n(k) + \hbar^2 k_y^2/2m$ where $E_n(k)$ exhibits a miniband structure similar to that shown in Fig. 4. As $|k_y|$ increases [in Fig. 4: (a) $k_y = 0$, (b) $k_y = 0.5$, (c) $k_y = 2$, and (d) $k_y = 5$] the lower bands become narrower and consequently the corresponding states are more lo-

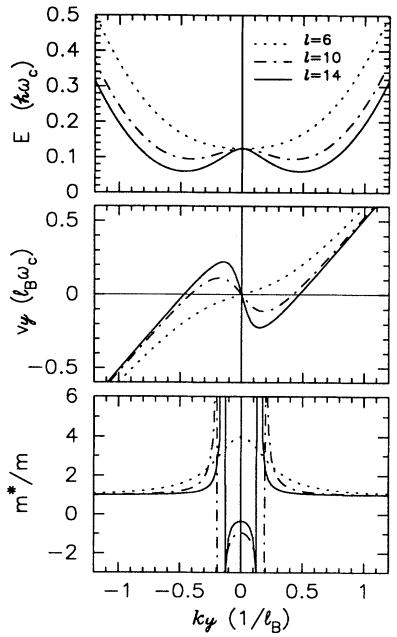

FIG. 7. The bottom of the lowest-energy band (top), the drift velocity (middle), and the effective mass (bottom) vs k_y for three different periodic lengths $l = 6, 10, 14$, for the MKP model.

calized in the x direction. This is clearly shown in the E versus k_y curves (Fig. 5) where the width of the shaded region corresponds to the height of the miniband along k (i.e., the x direction). Notice that the energy levels that are below the maximum of the potential have a very small miniband width [the minimum and maximum of the potential $V(x,k_y)$ are indicated by the dash-dotted curves in Fig. 5]. Electrons with large k_y correspond to states that are predominantly confined to move parallel to the y axis with vanishing v_x component (i.e., 1D wire states). Note that the states with motion in the $+y$ and $-y$ directions are localized in separate regions of the (x,y) plane, as can be easily inferred by looking at the potential profile $V(x,k_y)$ (see Fig. 3). Indeed, the potential wells for k_y values of opposite sign are separated by half a period $l/2$. Note that this behavior is similar to edge states in quantum wires in the presence of a perpendicular homogeneous magnetic field where the k_y and $-k_y$ edge channels are located at the opposite edges of the quantum wire.

The dependence of the energy spectrum on the period l is shown in Fig. 6 for a fixed k_y value. The areas between the bottom and top of the energy minibands are shaded. Notice that as the period increases the miniband width decreases and this leads to energy levels of isolated wells. The latter are well approximated by $(\pi^2\hbar^2/2ml^2)n^2 + V_{\min}$. In fact in this limit the problem reduces to the one of isolated quantum wires. From Figs. 5 (E versus k_y) and 6 (E versus l) we notice that bands cross at certain points. This degeneracy occurs when both αl and βl are integer multiples of π, which leads to $k = n\pi/l$, $E = [(n\pi/l)^2 + (|k_y| + 1/2)^2]/2$, with the integer $n \geq 1$. The physical meaning is that for those particular values of the energy, the period and the wave vector k_y, there is a Fabry-Pérot effect for the electron waves in both the well region and the barrier region.

From Fig. 5 and the inset of this figure, we notice a peculiar behavior of the energy spectrum around $k_y = 0$. To understand this we expand relation (7) in powers of k_y around $(k,k_y) = (0,0)$, which leads to

$$E(k=0,k_y) = a_0 + a_2k_y^2 + a_4k_y^4 + \cdots, \qquad (8)$$

where $a_0 = 1/8$, $a_2 = 1/2 - 0.01042l^2$, and $a_4 = 0.5167 \times 10^{-5}l^6$. For $l = 0$ the parabolic dispersion of the free 2DEG is regained. For $a_2 < 0$, which occurs when $l/\ell_B > 9.8$, the energy has a local maximum at $k_y = 0$ and a double minima at $k_y = \pm\sqrt{-a_2/2a_4}$ (see Fig. 7). At these three extremal points the drift velocity $v_y = \partial E/\partial k_y$ vanishes and it reverses its sign. The electron effective mass, $m^*/m = 1/(\partial^2 E/\partial k_y^2)$, exhibits a singular behavior as it changes its sign discontinuously from negative to positive at $k_y = \pm\sqrt{-a_2/6a_4}$, where the drift velocity v_y attains a local maximum (see Fig. 7).

Most of the qualitative features of the present system can be understood from a study based on classical trajectories. The classical equations of motion are $\dot{v}_x = -\omega_c v_y$ and $\dot{v}_y = \omega_c v_x$, where $\omega_c = eB/mc$. The interaction of the electron with our δ-function magnetic field profile results into a change of the direction of motion of the electron : $(v_x,v_y) \to (v_x',v_y')$ with $v = \sqrt{v_x^2+v_y^2} = v' = \sqrt{v_x'^2+v_y'^2}$. We have the following possibilities: (1) $v_x > 0$: (a) when $v_x^2 > 2v_y\omega_c + \omega_c^2$ we have transmission through the barrier with $v_y' = v_y + \omega_c$, while (b) $v_x^2 < 2v_y\omega_c + \omega_c^2$ results in reflection: $v_x' = -v_x$ and $v_y' = v_y$; (2) $v_x < 0$: (a) when $v_x^2 > \omega_c^2 - 2v_y\omega_c$ we have transmission with $v_y' = v_y - \omega_c$, while (b) $v_x^2 < \omega_c^2 - 2v_y\omega_c$ leads to reflection. For scattering with the opposite barrier $B = -B_0\delta(x)$ the results are similar as above, but now we should replace ω_c by $-\omega_c$.

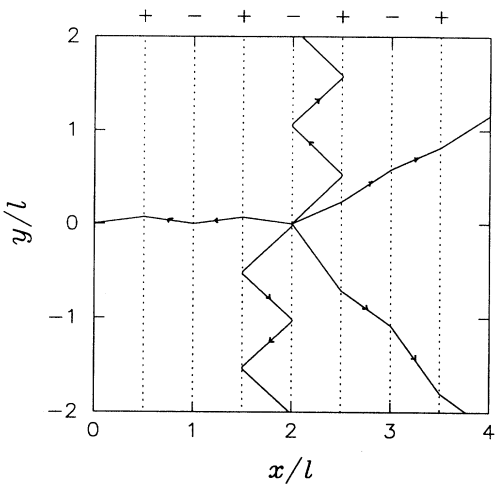

FIG. 8. Possible classical trajectories with the same initial position but different initial velocities for the MKP model. Two trajectories, which have energies below the barriers, are confined to move in two separate regions in x space but in opposite y directions and which have $\langle v_x\rangle = 0$.

In the case of our superlattice we find that in this classical treatment, the starting point of our electron is important whether or not we have reflection. For an initial position $0 < x < l/2$ (modulo l) and an initial velocity $\vec{v} = (v_x,v_y)$ we have reflection between the two barriers when $v_x^2 < -2\omega_c v_y + \omega_c^2$, which results in the average velocity $\langle\vec{v}\rangle = (0,v_y)$ and which corresponds to the flat bands in Fig. 4, while for $v_x^2 > -2\omega_c v_y + \omega_c^2$ there is transmission through all the barriers with average electron velocity $\langle v_x\rangle = \frac{1}{2}(v_x + \sqrt{v_x^2 + 2v_y\omega_c - \omega_c})$, $\langle v_y\rangle = v_y - \frac{1}{2}\omega_c$ when $v_x > 0$, and $\langle v_x\rangle = \frac{1}{2}(v_x + \sqrt{v_x^2 - 2v_y\omega_c - \omega_c})$, $\langle v_y\rangle = v_y + \frac{1}{2}\omega_c$ when $v_x < 0$. When the starting position is such that $l/2 < x < l$ (modulo l) we obtain similar results as above but with v_y replaced by $-v_y$. The possible classical trajectories are illustrated in Fig. 8 with a common starting position.

IV. PERIODIC STEP MAGNETIC FIELD

When in the physical system of Fig. 1 we consider the limit of a small distance between the 2DEG and the ferromagnetic thin film a periodic step magnetic field profile

is obtained. The electrons feel an abrupt change in the field direction without an appreciable change in magnitude [solid curve in Fig. 1(b)]. We consider the limit of a periodic step magnetic field

$$B(x)/B_0 = \sum_{n=-\infty}^{\infty} (-1)^n \theta(x - nl/2)\theta[(n+1)l/2 - x], \tag{9}$$

which results into the sawtooth vector potential, note that $B(x) = dA(x)/dx$,

$$A(x)/A_0 = \sum_{n=-\infty}^{\infty} (-1)^n [x - (2n+1)l/4] \times \theta(x - nl/2)\theta[(n+1)l/2 - x], \tag{10}$$

where $\theta(x)$ is the Heaviside step function. The profiles for $B(x)$ and $A(x)$ are depicted in Fig. 9 together with the effective potential for different k_y values. When solving the Schrödinger equation we can restrict ourselves to one period in which the vector potential is given by $A(x) = x - l/4$ ($0 \le x \le l/2$), $-x + 3l/4$ ($l/2 \le x \le l$). After making the following change of variable $X = \sqrt{2}[k_y + A(x)]$ the Schrödinger equation (4) is cast into the following form:

$$\left\{ \frac{d^2}{dX^2} + E - X^2/4 \right\} \psi(X) = 0, \tag{11}$$

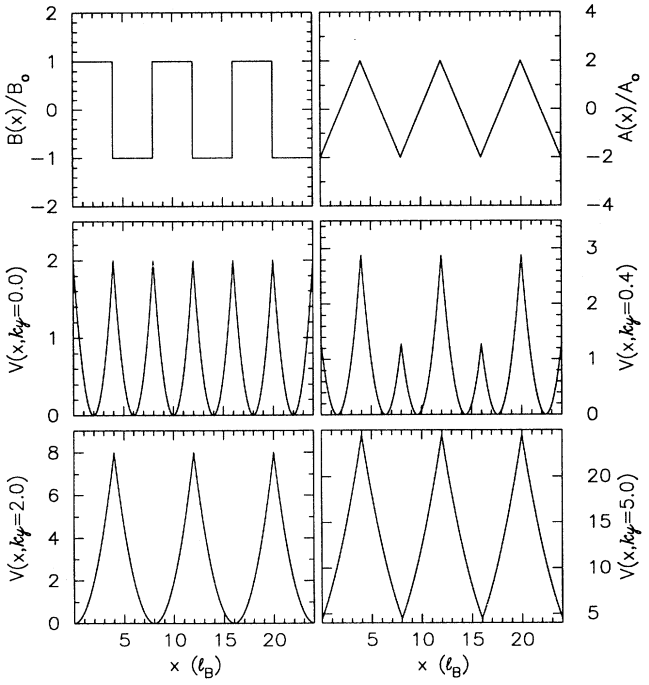

FIG. 9. The profiles for the magnetic field $B(x)$, the vector potential $A(x)$ and the effective potential $V(x, k_y)$ for k_y =0.0, 0.4, 2.0, 5.0 in the case of the periodic step model.

which is the parabolic cylinder equation. This equation has two linearly independent solutions $\psi_1(X) = e^{-X^2/4}\ {}_1F_1(-E/2 + 1/4, 1/2, X^2/2)$ and $\psi_2(X) = Xe^{-X^2/4}\ {}_1F_1(-E/2 + 3/4, 3/2, X^2/2)$ where ${}_1F_1(a, c; x)$ is the confluent hypergeometric function. Imposing the conditions of continuity and the Bloch periodicity on the wave function and its first derivative leads to the following transcendental equation for the energy momentum relation:

$$\cos(kl) = h(x_+)h(x_-) - 2[g_1(x_+)g_2(x_-) + g_2(x_+)g_1(x_-)]. \tag{12}$$

In Eq. (12) we defined $h(x) = \psi_1(x)\psi_2'(x) + \psi_2(x)\psi_1'(x)$, $g_i(x) = \psi_i(x)\psi_i'(x)$ and $x_\pm = \sqrt{2}(k_y \pm l/4)$.

The numerical solution of relation (12) for E versus k_y is shown in Fig. 10 for $l = 8$. In order to understand the energy spectrum we show in Fig. 9 the potential $V(x, k_y)$ for different k_y values. First, note that $V(x, k_y) = V(x + l/2, -k_y)$, which results in spatially separated motions for the $+k_y$ and $-k_y$ electrons moving with $E < V_{\max} = (|k_y| + l/4)^2/2$. For $k_y = 0$ the profile for $V(x, k_y)$ (see Fig. 9) is a periodic array of harmonic oscillators with finite depth ($= l^2/32$) and period $l/2$. In this case, the first Brillouin zone (FBZ) edge is at $k = 2\pi/l$ and gaps in the spectrum appear only at $k = 2n\pi/l$, where n is the band index. When k_y takes values different from zero the periodicity of $V(x, k_y)$ becomes twice as large and equals l and consequently the FBZ edge becomes $k = \pi/l$ and the number of energy bands and gaps doubles. For $0 < |k_y| < l/4$ the potential profile within one period consists of a double harmonic

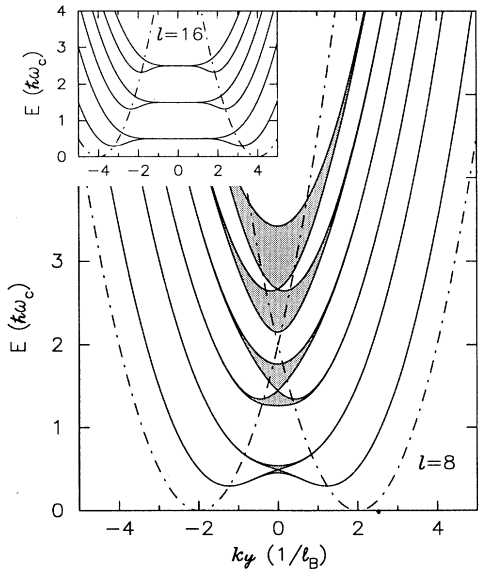

FIG. 10. Energy vs k_y dispersion relation for the periodic step model with $l = 8$. The shaded regions are the lowest six allowed energy bands. The dash-dotted curves show the maxima and minima of $V(x, k_y)$. Inset: The same for $l = 16$.

oscillator in which the middle barrier is smaller than the side barriers and decreases to zero at $|k_y| = l/4$ where $V(x, k_y)$ takes the shape of a single harmonic oscillator in one period with depth= $l^2/8$. The bands with energy below the barrier height, (the dash-dotted curves in Fig. 10 indicate the bottom and top of the potential profile), i.e., $E < V_{\max}$, correspond to open orbits traveling along the y direction and oscillating around the boundary separating the two magnetic strips. Electrons at adjacent boundaries move in the opposite y direction. For $|k_y| > l/4$, the profile $V(x, k_y)$ becomes increasingly V shaped with minima at $V_{\min} = (|k_y| - l/4)^2/2$ and maxima at $V_{\max} = (|k_y| + l/4)^2/2$. The 1D states below $V_{\max}$ are similar to the so-called magnetoelectric states (i.e., linear combinations of Airy functions). Here, also, the electron motion along the $\pm y$ directions are spatially separated by half a period $l/2$.

Figure 11 shows E vs l (at fixed $k_y = 2$), which illustrates the critical balance between k_y and $l/4$ and the concomitant dimensional transition from 0D closed-orbit Landau states present for large l (the homogeneous field limit) to the free 2DEG at $l = 0$ (zero field limit). In between the system passes through the 1D states (the inhomogeneous field regime) near $l/4 = k_y$, the value at which the center coordinate lies exactly on the boundary line separating the $+B_0$ and $-B_0$ regions, which results into the open-orbit states. For $|k_y| = l/4$, we have $V_{\min} = 0$ and the separation between the energy levels equals $\hbar\omega_c$. Notice that for $l \to \infty$ we recover the homogeneous field limit $E = (n + 1/2)\hbar\omega_c$, which is essentially different from the result for the MKP model where the energies of a particle in a box were obtained. The twofold degeneracy of levels for $k_y << l/4$ (see inset of Fig. 10 and Fig. 11 for large l) can be understood as follows: for the lower-energy states when $k_y \ll l/4$ the cyclotron orbit of the electron is completely contained within the boundaries of a single domain strip. In one period we have two domain strips, one with $+B_0$ and the

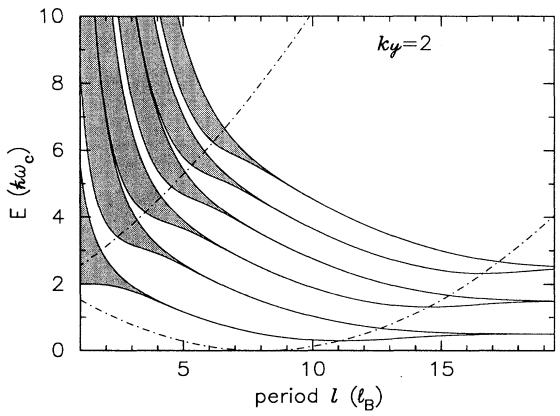

FIG. 11. Energy vs periodic length l at a fixed $k_y = 2$. The shaded regions are the allowed energy bands of which only the lowest six are shown. The dash-dotted curves are the maxima and minima of $V(x, k_y)$.

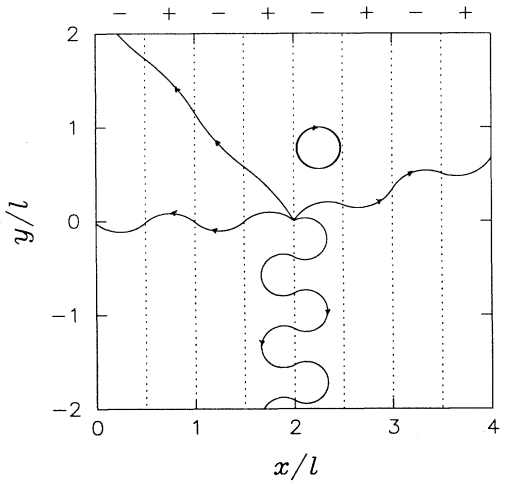

FIG. 12. Possible classical trajectories with the same initial position but different initial velocities for the periodic step model.

second with $-B_0$, and for the same energy the electron traverses the cyclotron orbit in one direction in the first strip and in the opposite direction in the second strip, hence the twofold degeneracy of this energy state. At larger k_y values the center coordinate of both cyclotron orbits becomes close to the boundary line between $+B_0$ and $-B_0$, and the electron states become open orbits that are traveling states wiggling around the boundary line. Now, the potential profile $V(x, k_y)$ in one period becomes a double harmonic oscillator with two minima and a middle barrier that is smaller than the side barriers. When the energy of the electron is close to the top of the middle barrier tunneling between the two regions becomes possible, resulting in the energy splitting of the originally degenerate energy states (see inset of Fig. 10). Because the strength of the middle barrier depends on the value of k_y this splitting occurs at different k_y values for the different energy bands.

In Fig. 12 samples of the three kinds of possible classical orbits are given: (1) 0D cyclotron motion, which occurs when the electron energy is sufficiently small that its cyclotron diameter is less than the width of the magnetic strip. This state is absent in the MKP system. (2) 1D drift parallel to the magnetic strips for states with the center of their cyclotron orbit near the interface between the $+B_0$ and $-B_0$ regions. (3) 2D motion in the plane when the electron energy is larger than the magnetic field barriers which results in a cyclotron diameter larger than the width of the magnetic strips.

V. SINUSOIDAL MAGNETIC FIELD

The physical system depicted in Fig. 1 has a sinusoidal magnetic-field profile in the plane of the 2DEG when the distance between the 2DEG and the ferromagnetic thin film is sufficiently large [see dotted curve in Fig. 1(b)]. In such a case only the first term of the Fourier series is

important. In this section we study the magnetic field profile

$$B(x)/B_0 = \sin(2\pi x/l), \tag{13}$$

which has the corresponding vector potential (Fig. 13)

$$A(x)/A_0 = -\frac{l}{2\pi}\cos(2\pi x/l), \tag{14}$$

and which leads to the following Schrödinger equation:

$$\left\{\frac{d^2}{dx^2} + 2E - [k_y - \frac{l}{2\pi}\cos(2\pi x/l)]^2\right\}\psi(x) = 0. \tag{15}$$

After making the substitutions $\theta = \pi x/l$, $\omega = (l/\pi)^2$, $\rho = lk_y/\pi$ and $\eta = (l/\pi)^2(2E - k_y^2 - 1/4)$, the above equation is cast into the following form

$$\left\{\frac{d^2}{d\theta^2} + [\eta + (\omega^2/8) + \omega\rho\cos(2\theta) - (\omega^2/8)\cos(4\theta)]\right\}\psi(\theta) = 0, \tag{16}$$

which is the Wittaker-Hill equation for which a detailed treatment can be found in Ref. 17. It is interesting to note that in the case $k_y = 0$ Eq. (16) reduces to Mathieu's equation with period $l/2$. At the end we are interested in numerical results and therefore, we used the method of Ref. 18. The latter technique relies on rewriting the above Schrödinger equation as a difference equation, which results in a continued fraction expression for the energy dispersion relation. Explicitly, it is given by

$$\cos(kl) = \tfrac{1}{2}[A_{n+1}(2E) - B_{n-1}(2E)], \tag{17}$$

where the coefficients A_n and B_n are determined by the recurrence relations $A_n(2E) = b_n(2E)A_{n-1}(2E) - A_{n-2}(2E)$ and $B_{n-1}(2E) = b_n(2E)B_{n-2}(2E) - B_{n-3}(2E)$ with the initial conditions $A_0(2E) = 1$, $B_0(2E) = 1$, $A_1(2E) = b_1(2E)$ and $B_1 = b_2(2E)$ where $b_n(2E) = 2 + h^2[2V(x_n, k_y) - 2E]$ and $h = l/(n+1)$. The period $l = x_{n+1} - x_0$ is divided into $n+1$ subintervals.

The wave function can be constructed according to the prescription of Ref. 17 once the energy spectrum is obtained. The potential profile $V(x, k_y)$ is shown in Fig. 13 where we have $V(x, k_y) = V(x + l/2, -k_y)$. This system is in many respects similar to the periodic magnetic step system discussed earlier. This is also apparent from the energy dispersion relation; i.e., compare Fig. 10 and Fig. 14. The same qualitative discussion holds for both systems and therefore we refer to the previous section for it. Possible classical trajectories are given in Fig. 15 (see also Ref. 19) where the similarity with the periodic step

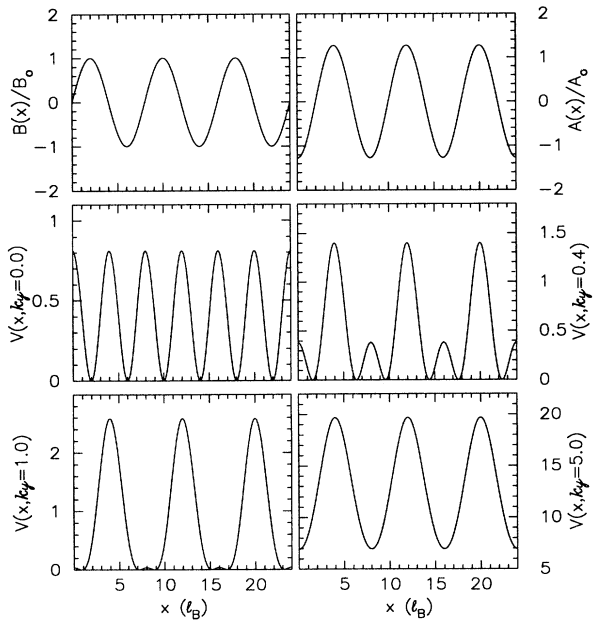

FIG. 13. The profiles for the magnetic field $B(x)$, the vector potential $A(x)$ and $V(x, k_y)$ for k_y =0.0, 0.4, 1.0, 5.0 in the case of the sinusoidal magnetic field model.

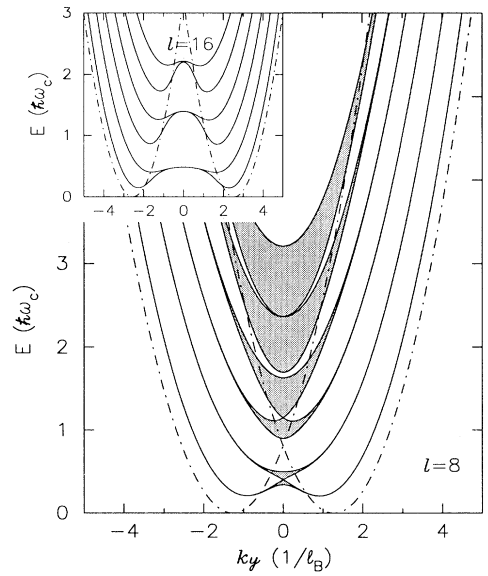

FIG. 14. Energy vs k_y dispersion relation for the sinusoidal field model with $l = 8$. The shaded regions are the lowest six allowed energy bands. The dash-dotted curves show the maxima and minima of $V(x, k_y)$. Inset: The same for $l = 16$.

system is obvious. But notice that now, e.g., the fully closed cyclotron orbit is no longer a circle.

VI. SAWTOOTH MAGNETIC FIELD

The system considered in Ref. 4 is a 2DEG, which is constrained by rigid walls in the x direction $|x| = l/2$, but which is infinite along the y axis. A nonhomogeneous magnetic field $B(x) = B_0 x$ directed perpendicular to the (x, y) plane was applied. Here we make a superlattice out of this system by removing the rigid-wall condition and repeating the geometry indefinitely along the x axis. Thus we consider the following magnetic field profile

$$B(x)/B_0 = (2/l) \sum_{n=-\infty}^{\infty} [x - (n + 1/2)l]\theta[x - (n + 1)l]\theta(x - nl), \tag{18}$$

with the corresponding vector potential

$$A(x)/A_0 = (1/l) \sum_{n=-\infty}^{\infty} [x - (n + 1/2)l]^2\theta[x - (n + 1)l]\theta(x - nl), \tag{19}$$

which are depicted in Fig. 16. Because of Bloch's theorem, the Schrödinger equation (4) has only to be solved within one period, which reduces to the finite anharmonic oscillator problem

$$\left\{ \frac{d^2}{dx^2} + 2E - (k_y + x^2/2)^2 \right\} \psi(x) = 0, \tag{20}$$

with a quartic anharmonicity term $x^4/4$. To generate the energy spectrum, we again made use of the method of Ref. 18. Once the energy spectrum is found the wave function can be obtained by substituting $\psi(x) = e^{-x^2/2} \sum_{n=0}^{\infty} c_n x^n$ into the above equation, which yields a recurrence relation for the coefficients c_n, which can be determined iteratively.[20]

It is not easy to imagine how to realize this system experimentally. One possibility is to use the technique suggested in Ref. 6 where either the ferromagnetic thin film or the semiconductor interface containing the 2DEG is grown on an etched substrate in such a way that the distance between the 2EG and the ferromagnetic thin film is varied periodically to produce the desired magnetic field profile in the 2DEG. Alternatively, regrowth techniques as used in, e.g., Ref. 14 can be used on a patterned substrate with a parabolic periodic profile. When a magnetic field is applied parallel to the x axis and a 2DEG is grown with a topography that is a periodic rep-

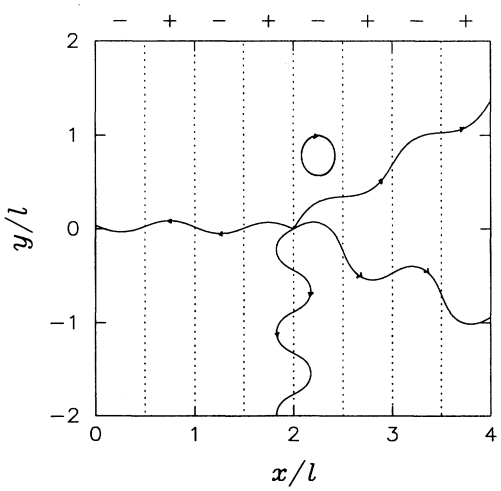

FIG. 15. Possible classical trajectories with the same initial position but different initial velocities for the sinusoidal field model.

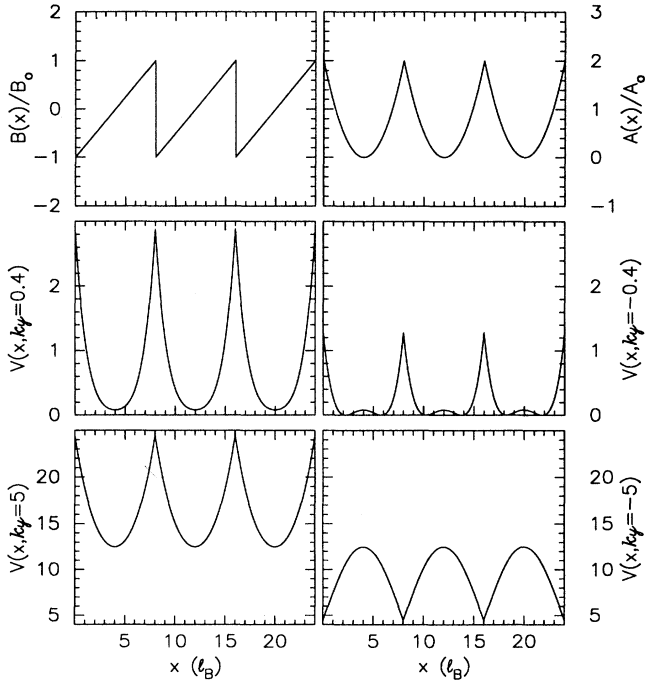

FIG. 16. The profiles for the magnetic field $B(x)$, the vector potential $A(x)$ and $V(x, k_y)$ for k_y =0.4, −0.4, 5.0, −5.0 in the case of the sawtooth magnetic field model.

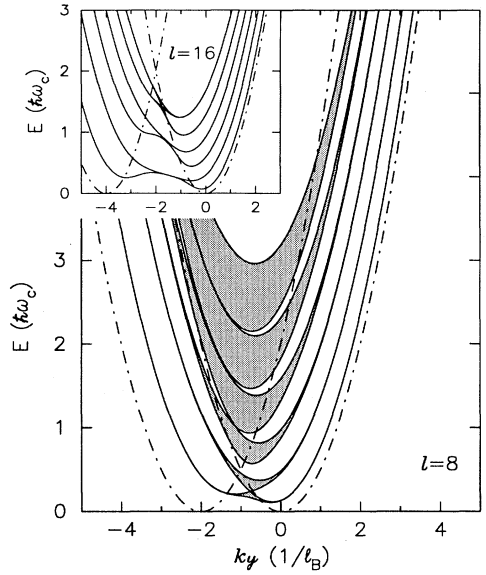

FIG. 17. Energy vs k_y dispersion relation for the sawtooth field model with $l = 8$. The shaded regions are the lowest six allowed energy bands. The dash-dotted curves show the maxima and minima of $V(x, k_y)$. Inset: The same for $l = 16$.

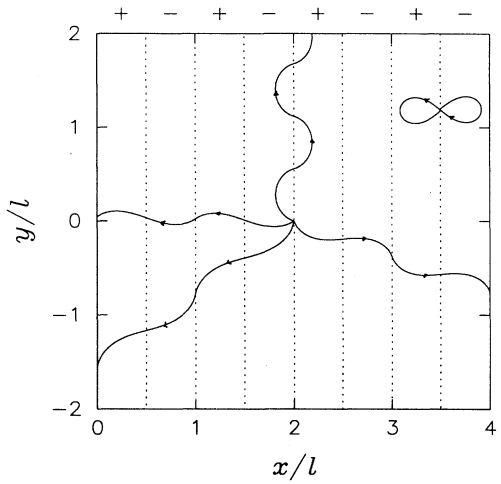

FIG. 18. Possible classical trajectories with the same initial position but different initial velocities for the sawtooth field model.

etition of the profile $h(x, y) = ax^2$, $|x| < l/2$, will lead to the above effective magnetic field normal to the 2DEG.

The magnetic field profile is now no longer invariant under spatial inversion. As a consequence the effective potential $V(x, k_y)$, displayed in Fig. 16, is asymmetric with respect to k_y. Therefore, the dispersion relation for E versus k_y is no longer symmetric (see Fig. 17) for $k_y \to -k_y$, in other words, electrons moving in opposite y directions no longer have the same energy.

Notice in Fig. 16 the large difference in effective potential for electrons moving in the positive k_y direction (left figures) and electrons moving in the negative k_y direction (right figures). For large $|k_y|$ values the effective potential for $k_y > 0$ consists of a periodic area of harmonic potentials while for $k_y < 0$ they are inverse parabolas. It is therefore not surprising that the electron motion in such two superlattices will be very different. Also the minima of the corresponding potentials are located at different positions in space and consequently also the corresponding probability maxima in the electron wave function. Electrons with energies below the barriers and with positive k_y are localized in regions where the magnetic field changes continuously from negative to positive and electrons with negative k_y are localized in regions where the sign of the magnetic field changes discontinuously. Notice that within the same energy miniband, electrons with positive k_y are in a higher-energy state than electrons with equal and opposite k_y.

Besides the $k_y \to -k_y$ asymmetry in the energy spectrum there are two other important differences as compared with previous cases: (1) the minibands are wider for $k_y < 0$. This can be understood from Fig. 16 where we see that the superlattice potential for $k_y < 0$ is shallower than for $k_y > 0$. The implication of wider minibands is that the corresponding electron states can more easily propagate in the x direction, thus having a larger v_x; (2) even for cases with large l values (see inset of Fig. 17) the energy spectrum does not have a flat region near $k_y = 0$ as in previous cases (see inset of Figs. 10 and 14). We notice that for $k_y < 0$ and for large l-values the energy bands become twofold degenerate: symmetric and asymmetric states have the same energy for those k_y-values. This is a similar effect which was observed in the equivalent 1D-case with rigid walls (see Ref. 4). For large values of the period l and not too large energy the system of Ref. 4 is a limiting case of the present system. Possible classical trajectories are depicted in Fig. 18. Now the 0D state is no longer a circle as in the periodic step profile or an ellipse as for the sinusoidal case but an orbit that has the shape of the number eight.

VII. DENSITY OF STATES AND CONDUCTIVITIES

The zero-temperature density of states (DOS) for the systems considered is calculated by numerically integrating the inverse of the magnitude of the energy gradient in momentum space along the constant-energy contours at the Fermi energy and within the first Brillouin zone

$$D(E)/D_0 = (1/2\pi) \sum_n \int_{S_n} \frac{dS_n}{|\nabla E_n(k)|}, \qquad (21)$$

where $D_0 = m^*/\pi\hbar^2$ is the DOS of the free 2DEG, n is the band index, and S_n is the constant-energy contour. Spin splitting of the energy levels is neglected. The spin degeneracy is taken into account and no scattering is assumed other than the interaction with the magnetic field.

The diagonal components of the electric conductiv-

ity tensor are calculated concurrently with the DOS and along the same constant energy contours where we used the expression

$$\sigma_{ii}/\sigma_0 = \sum_n \int_{S_n} v_{n,i} v_{n,i} dS_n, \tag{22}$$

with $v_{n,i} = \partial E_n/\partial k_i$ the drift velocity and σ_o is the Drude conductivity of the free 2DEG. This formula is valid for diffusive type of transport at zero temperature. Notice that because there is no net magnetic field, i.e., $\langle B \rangle = 0$, we do not expect any Hall resistance and consequently $\sigma_{xy} = 0$.

The density of states for the MKP system (Fig. 19) is predominantly a free 2DEG except for singular points: (1) resulting from the edges of the minibands, which occur for $k_x = (2n+1)\pi/l$, $n = 0, 1, 2, 3, \ldots$, and (2) resulting from the local minima in the energy spectrum (see Fig. 5), which occur for small k_y values where $v_y = 0$. At these points in momentum space the conditions for Bragg reflection are met for motion in the x direction and the average velocity in the y direction is zero. Electrons with these energies and wave vectors form standing waves with zero average velocity. This effect results in dips in the σ_{xx} conductivity (Fig. 19). Note that no such clear structure is apparent in the σ_{yy} conductivity because motion in the y direction does not exhibit this Bragg reflection. Between the dips, σ_{xx} exhibit local peaks at which $\sigma_{xx} \approx \sigma_{yy}$. This is easily understood from Fig. 5 where we see that at those energy values minibands touch each other and the energy gap between the inner minibands disappear. As a consequence, for those energy values the effect of the periodic magnetic field on the electron motion is minimal and consequently the difference between σ_{xx} and σ_{yy} will be minimal.

The energy spectrum, the density of states, and the diagonal components of the conductivity tensor for the periodic step model are depicted in Fig. 20. The structure

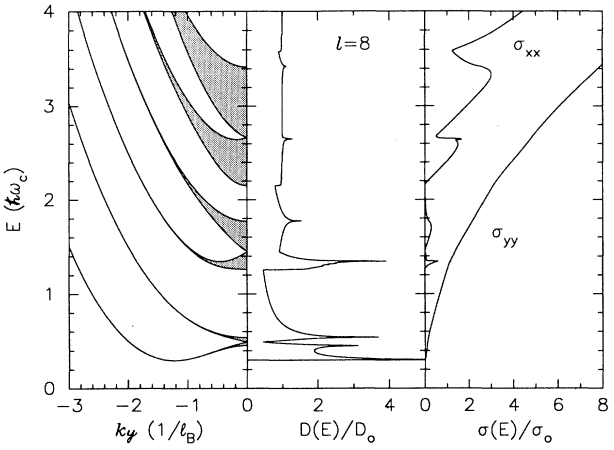

FIG. 20. The energy dispersion curves (left panel), the density of states (middle panel), and the diagonal components of the electric conductivity tensor (right panel) for the periodic step system for $l = 8$.

in the DOS can be understood in the light of the E versus k_y relation. The first singularity in $D(E)$ occurs at the onset of the allowed energy bands and corresponds to 1D states [notice that the miniband width (shaded area) is zero] where motion is only possible along the y direction and consequently $\sigma_{xx} = 0$. The second and third peaks in the DOS, which are symmetric about $\frac{1}{2}\hbar\omega_c$, originate from the edges (saddle points) of the lowest Landau level, which is broadened by the finite tunneling to neighboring strips. Beyond the third peak there are no states available for motion along the x direction because of the energy gap where motion is possible only along the y direction and consequently $\sigma_{xx} \approx 0$. For larger energies the structure in the DOS gradually diminishes due to the enhanced tunneling probability near the top of the barriers and the availability of 2D states above the barriers where

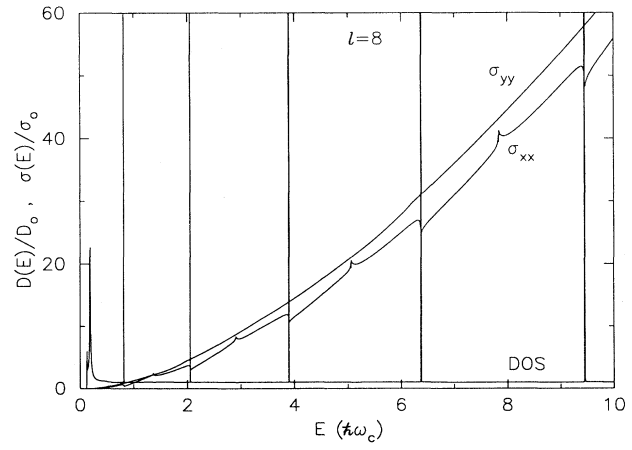

FIG. 19. The density of states and the diagonal components of the electric conductivity tensor vs Fermi energy for the magnetic Kronig-Penney system with $l = 8$.

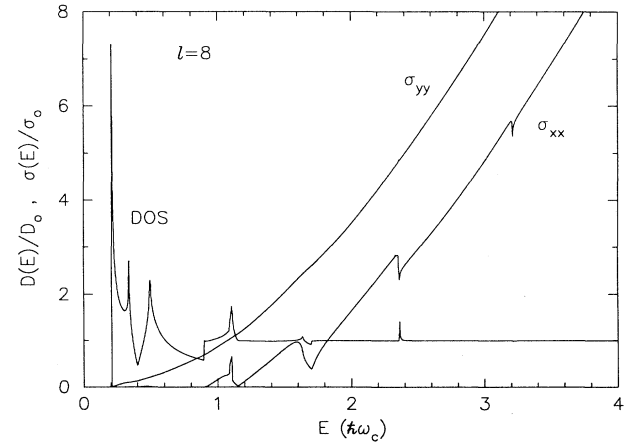

FIG. 21. The density of states and the diagonal components of the electric conductivity tensor vs Fermi energy for the sinusoidal system with $l = 8$.

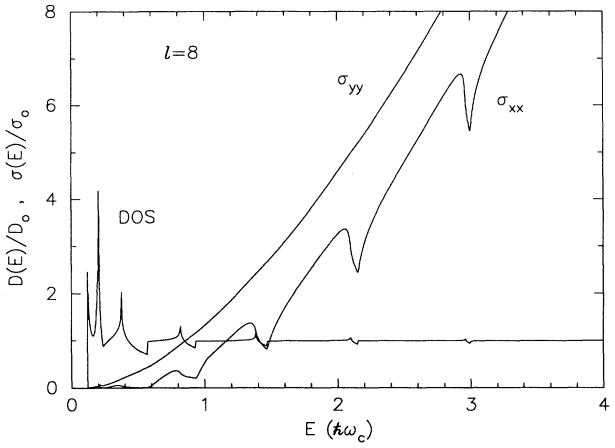

FIG. 22. The density of states and the diagonal components of the electric conductivity tensor vs Fermi energy for the sawtooth system with $l = 8$.

the DOS approaches its limiting value for the free 2DEG. In this case motion along the x direction is possible and σ_{xx} becomes substantially different from zero. Note that we always have $\sigma_{xx} < \sigma_{yy}$.

The DOS and σ_{ii} for the sinusoidal system (Fig. 21) are seen to have a structure closely resembling that of the periodic step system. In Ref. 21 these quantities were already calculated using different techniques. Our results are very similar and therefore we refer to Ref. 21 for a discussion of it.

The sawtooth case (Fig. 22) can also be understood in terms of its E versus k_y dispersion relation where the structure in the DOS consists of energy regions dominated by the contributions of the 2D states (the shaded areas in E versus k_y) alternating with energy regions where the dominant contribution is from 1D states corresponding to the energy gaps between the shaded regions. At high energies the DOS for all systems considered converge to D_0 the DOS for the free 2DEG.

In general, we found that the components of the electrical conductivity tensor σ_{ii} versus the Fermi energy show a universal behavior in all of the systems considered. The σ_{yy} conductivity is obviously the least affected by the presence of the magnetic field modulations along the x direction, since there are always states available for motion along the y direction regardless of the Fermi energy. Furthermore, the number of these states increases with increasing energy. In contrast, the miniband structure has a pronounced effect on the σ_{xx} component due to the existence of energy gaps for motion along the x direction, where σ_{xx} shows downward dips corresponding to the edges of the Brillouin zone where $v_x \approx 0$. The magnitude of σ_{xx} does not become appreciable until the Fermi energy is near or above the magnetic potential barrier at $k_y = 0$. The σ_{xx} is always less than σ_{yy} even for high energies. The reason is that the effect of Bragg reflections, which does not influence σ_{yy}, persists up to high energies, which is a purely quantum-mechanical effect.

VIII. CONCLUSION

We have investigated the energy spectrum for a 2DEG in a periodically modulated magnetic field along one direction with zero average in the plane (ferromagnetic arrangement). It is shown that many features of these systems are different from the electrostatically modulated ones or the ones considered in Refs. 7–9 with a constant background magnetic field. For example, the bandwidths, the effective mass, and the drift velocity along the y direction all have a k_y dependence. The periodicity of the effective potential $V(x, k_y)$ may change or completely vanish at $k_y = 0$ with the corresponding reduction or disappearance of energy gaps. Depending on the value of the periodic length the lowest-energy bands may have double minima at a finite value of k_y where the drift velocity can be zero and the effective mass may exhibit a divergent behavior. The density of states and components of the electric conductivity tensor were also calculated for these systems. They exhibit a structure that is related to the behavior of the electrons near the edges of the magnetic minibands. σ_{yy} is not much influenced while σ_{xx} exhibits a strong increase each time the Fermi energy crosses a new magnetic miniband. At the upper edge of this miniband σ_{xx} decreases substantially. In all cases we found $\sigma_{xx} < \sigma_{yy}$.

ACKNOWLEDGMENTS

One of us (F.M.P.) is supported by the Belgian National Science Foundation. Part of this work is funded by the Interuniversity Microelectronics Center (IMEC, Leuven).

APPENDIX

We calculate the magnetic field resulting from a ferromagnetic thin film in which the magnetic domains are in the form of a periodic array of parallel strips [see Fig. 1(a)]. The magnetization of each domain strip can either be in the plane of the film or perpendicular to it. Since no currents are involved, Maxwell's equations are

$$\vec{\nabla} \cdot \vec{B} = 0, \quad \vec{\nabla} \times \vec{H} = 0, \tag{A1}$$

where $\vec{B} = \mu_0(\vec{H} + \vec{M})$ and $\vec{M}$ is the magnetization. $\vec{H}$ can be written in terms of the gradient of a scaler potential $\vec{H} = -\vec{\nabla}\Phi_m$, which leads to

$$\nabla^2\Phi_m = -\vec{\nabla} \cdot \vec{H} = \vec{\nabla} \cdot \vec{M}. \tag{A2}$$

If we define a magnetic charge density by $\rho_m = -\vec{\nabla} \cdot \vec{M}$, the above equation leads to Poisson's equation

$$\nabla^2\Phi_m = -\rho_m, \tag{A3}$$

which can be solved by the standard methods of electrostatics. The magnetic field can be given directly by Coulomb's law

$$\vec{B}(\vec{r}) = \frac{\mu_0 M}{4\pi} \int d\vec{r}\,' \frac{\rho_m(\vec{r}\,')(\vec{r}-\vec{r}\,')}{|\vec{r}-\vec{r}\,'|^3}. \quad \text{(A4)}$$

First, we consider the case depicted in Fig. 1(a) but where we consider only a single magnetic domain strip with magnetization perpendicular to the (x,y) plane with boundaries $x \in (-a,a), y \in (-\infty,\infty), z \in (-d,d)$, which implies

$$\rho_m = -\nabla \cdot \vec{M} = M[\delta(z-d) - \delta(z+d)] \times[\theta(x+a) - \theta(x-a)], \quad \text{(A5)}$$

and the magnetic field at the point $\vec{r}$ is obtained from Eq. (A4) as

$$\vec{B}(\vec{r}) = \frac{\mu_0 M}{2\pi}[\vec{B}_*(x,y,z+d) - \vec{B}_*(x,y,z-d)], \quad \text{(A6)}$$

where

$$\vec{B}_*(\vec{r}) = \frac{1}{2}\ln\left(\frac{(x+a)^2+z^2}{(x-a)^2+z^2}\right)\vec{e}_x + \left[\arctan\left(\frac{x+a}{z}\right) - \arctan\left(\frac{x-a}{z}\right)\right]\vec{e}_z. \quad \text{(A7)}$$

For in-plane magnetization the solution can be obtained by simply rotating the magnetic strip by 90° about the y axis with the corresponding interchange of the x and z coordinates in the previous expression for the magnetic field; i.e., Eq. (A6) and (A7) become, respectively,

$$\vec{B}(\vec{r}) = \frac{\mu_0 M}{2\pi}[\vec{B}_*(x+a,y,z) - \vec{B}_*(x-a,y,z)], \quad \text{(A8)}$$

where

$$\vec{B}_*(\vec{r}) = \frac{1}{2}\ln\left(\frac{x^2+(z+d)^2}{x^2+(z-d)^2}\right)\vec{e}_z + \left[\arctan\left(\frac{z+d}{x}\right) - \arctan\left(\frac{z-d}{x}\right)\right]\vec{e}_x. \quad \text{(A9)}$$

The magnetic field profile resulting from a periodic array of ferromagnetic domain strips is the superposition of the contributions of each of the individual domain strips at that point. In particular for the situation of Fig. 1(a) we have

$$\vec{B}_{\text{total}}(\vec{r}) = \sum_{n=-\infty}^{\infty} (-1)^n \vec{B}[x - nl/2, y, z], \quad \text{(A10)}$$

where $\vec{B}(\vec{r})$ is given by Eq. (A6) and the period $l = 4a$. Using Poisson's method for the summation of infinite series we can write the z component of this expression also as

$$\vec{B}_z(\vec{r}) = \sum_{n=0}^{\infty} \vec{B}_n(k_n z)\cos(k_n x), \quad \text{(A11)}$$

with

$$\vec{B}_n(kz) = \frac{(-1)^n}{(2n+1)}(e^{-kd} - e^{kd})e^{-kz}\vec{e}_z, \quad \text{(A12)}$$

where $k_n = (2n+1)2\pi/l$. This result agrees with the solution obtained directly from Poisson's equation (A3) using the Fourier series expansion for ρ_m and the method of separation of variables. The resulting magnetic field profile is shown in Fig. 1(b) for different values of the distance z_0 from the area of the magnetic strips.

In the case the magnetic domains are aligned in the plane, but with alternating direction, we have

$$\vec{B}_{\text{total}}(\vec{r}) = \sum_{n=-\infty}^{\infty} (-1)^n \vec{B}[x - nl/2, y, z], \quad \text{(A13)}$$

but where $\vec{B}(\vec{r})$ is now given by Eq. (A8). Using Poisson's summation method we find the z component to be

$$\vec{B}_z(\vec{r}) = \sum_{n=0}^{\infty} \vec{B}_n(k_n z)\sin(k_n x), \quad \text{(A14)}$$

with k_n and $\vec{B}_n(kz)$ identical as given above. The resulting magnetic field profile is shown in Fig. 1(c) for different values of the distance z_0 from the area of the magnetic strips.

* Electronic address: peeters@uia.ua.ac.be

[1] F. M. Peeters and A. Matulis, Phys. Rev. B **48**, 15 166 (1993).

[2] A. Matulis, F. M. Peeters, and P. Vasilopoulos, Phys. Rev. Lett. **72**, 1518 (1994).

[3] V. M. Ramaglia, A. Tagliacosso, F. Ventriglia, and G. P. Zucchelli, Phys. Rev. B **43**, 2201 (1991); V. M. Ramaglia, and F. Ventriglia, J. Phys. Condens. Matter **3**, 4881 (1991).

[4] J. E. Müller, Phys. Rev. Lett. **68**, 385 (1992).

[5] M. Calvo, Phys. Rev. B **48**, 2365 (1993); J. Phys. Condens. Matter **6**, 3329 (1994); Phys. Rev. B **51**, 2268 (1995).

[6] C. L. Foden, M. L. Leadbeater, J. H. Burroughes, and M. Pepper, J. Phys. Condens. Matter **6**, L127 (1994).

[7] F. M. Peeters and Vasilopoulos, Phys. Rev. B **47**, 1466 (1993); P. Vasilopoulos and F. M. Peeters, Superlatt. Microstruct. **7**, 393 (1990).

[8] D. P. Xue and G. Xiao, Phys. Rev. B **45**, 5986 (1992).

[9] X. G. Wu and S. E. Ulloa, Solid State Commun. **82**, 945 (1992).

[10] H. A. Carmona, A. K. Geim, A. Nogaret, P. C. Main, T. J. Foster, M. Henini, S. P. Beaumont, and M. G. Blamire, Phys. Rev. Lett. **74**, 3009 (1995); P. D. Ye, D. Weiss, R. R. Gerhardts, M. Seeger, K. von Klitzing, K. Eberl, and H. Nickel, *ibid.* **74**, 3013 (1995); S. Isawa, S. Katsumoto, A. Endo, and Y. Iye, J. Phys. Soc. Jpn **64**, 706 (1995).

[11] W. Kang, H. L. Stormer, L. N. Pfeiffer, K. J. Boldwin, and K. W. West, Phys. Rev. Lett. **71**, 3850 (1993); R. L. Willet, R. R. Ruel, K. W. West, and L. N. Pfeiffer, *ibid.* **71**, 3846 (1993).

[12] A. Khaetskii and G. E. Bauer, Phys. Rev. B **51**, 7369

(1995); L. Brey and C. Tejedor, *ibid.* **51**, 17 259 (1995).
[13] W. Van Roy, J. De Boeck, and G. Borghs, Appl. Phys. Lett. **61**, 3056 (1992).
[14] M. L. Leadbeater, C. L. Foden, T. M. Burke, J. H. Burroughes, M. P. Grimshaw, D. A. Ritchie, L. L. Wang, and M. Pepper, J. Phys. Condens. Matter **7**, L307 (1995).
[15] P. P. Vil'ms and M. V. Éntin, Fiz. Tekh. Poluprovodn. **22**, 1905 (1988) [Sov. Phys. Semicond. **22**, 1209 (1988)].
[16] I. S. Ibrahim and F. M. Peeters, Am. J. Phys. **63**, 171 (1995). Please note that the k_y scale in Figs. 2, 4, and 6 should be in units of $1/l_B$.
[17] K. M. Urwin and F. M. Arscott, Proc. R. Soc. Edinburgh A **69**, 28 (1970).
[18] J. P. Vigneron and Ph. Lambin, J. Phys. A **12**, 1961 (1979).
[19] J. M. Repko, W. W. Repko, and A. Saaf, Am. J. Phys. **59**, 652 (1991).
[20] V. Singh, S. N. Biswas, and K. Datta, Phys. Rev. D **18**, 1901 (1978). See also Ref. 4 therein.
[21] R. B. S. Oakeshott and A. MacKinnon, J. Phys. Condens. Matter **5**, 9355 (1993).